

Integrated Predictive Modelling of JET H-mode Plasma with Type-I ELMs

V. Parail¹, G. Bateman², M. Becoulet³, G. Corrigan¹, D. Heading¹, J. Hogan⁴, W. Houlberg⁴, G.T.A. Huysmans³, J. Kinsey², A. Korotkov¹, A. Kritiz², A. Loarte⁵, J. Lonnroth⁶, D. McDonald¹, P. Monier-Garbet³, T. Onjun², G. Saibene⁵, R. Sartori⁵, S.E. Sharapov¹, H.R. Wilson¹ and JET-EFDA contributors.

¹ EURATOM/UKAEA Fusion Association, Culham Science Centre, Abingdon OX14 3DB, United Kingdom;

² Lehigh University, 16 Memorial Drive East, Bethlehem, PA 18015 USA;

³ Association Euratom-CEA, Cadarache 13108 SAINT PAUL LEZ DURANCE, FRANCE;

⁴ Oak Ridge National Laboratory, P.O. Box 2009, MS 8071, USA;

⁵ EFDA CSU – Garching, D85748 Garching, Germany;

⁶ Association EURATOM-TEKES, Helsinki University of Technology, P.O. Box 2200, FIN-02015 HUT, Finland

e-mail contact of main author: vparail@jet.uk

Abstract. Edge plasma parameters influence plasma performance in many different ways (profile stiffness is probably one of the best known examples). In ELMy H-mode, a thin region with improved transport characteristics (Edge Transport Barrier) links the core and the scrape-off layer. There is a strong coupling between these three areas, so that even a modest variation of plasma parameters in one region can lead to a dramatic change in the overall plasma performance. Systematic MHD stability analysis and self-consistent integrated predictive modelling of a series of JET ELMy H-mode plasmas, including scans in gas fuelling and triangularity are presented.

1. Introduction

Self-consistent integrated predictive modelling of ELMy H-mode plasma ideally should include simulation of the evolution of plasma parameters in the core, within the edge transport barrier (ETB) and in the scrape-off layer (SOL). Transport modelling should be complemented by the MHD stability analysis and further simulation of edge localised MHD instabilities (ELMs). The failure of dealing with one of the above-mentioned ingredients seriously undermines the understanding of the underlying physical processes and can lead to a loss of predictability. The paper deals with few characteristic examples of a strong link between core transport, ETB and SOL: the effect of strong gas puffing and of magnetic configuration on the performance of type-I ELMy H-mode.

2. Background experimental information

We have selected four recent JET ELMy H-mode plasmas, which constitute a scan in gas puff and in triangularity. All discharges have very similar level of plasma current $I_p \cong 2.5\text{MA}$, toroidal magnetic field $B_T \cong 2.6\text{T}$, ellipticity $\kappa \cong 1.7$ and the level of additional heating, provided by NBI: $P_{\text{NBI}} \cong 15\text{MW}$. Two discharges belong to a triangularity scan (#53186 has $\delta \cong 0.3$ and #53298 has $\delta \cong 0.5$) and three shots ##53298, 53299 and 52739 constitute gas-puffing scan (with $\Gamma = 0$ for #53298, $\Gamma \cong 4.5e22\text{ 1/sec}$ for #53299 and $\Gamma \cong 6e22\text{ 1/sec}$ for #52739). Figure 1 shows the time evolution of the energy content for these shots together with the $D\alpha$ signal and energy confinement time normalised to the H-mode scaling (H98y). At least two conclusions can be drawn from this figure:

1. Plasma with higher triangularity has better performance (in terms of both plasma stored energy and normalised confinement) than similar low triangularity plasma;
2. Strong gas puffing leads to a significant increase in ELM frequency (followed by transition to type-III ELMy H-mode in extreme cases). This leads to a noticeable degradation in plasma performance. It is worth noting that intermediate level of gas puffing can lead to a decrease of ELM frequency and transition to a mixed type I-II ELMy H-mode (see #53299) [5].

We will also discuss the possible cause of a sudden transition from type-I to type-III ELMs, observed in many experiments with a modest level of heating power [1], and try to associate the transition with a bifurcation in the edge MHD instability.

Transport models, codes and other tools used in integrated predictive modelling.

As we discussed earlier, there is a strong link between core transport and plasma parameters within the ETB and the SOL. To take this coupling into consideration we use a suite of JET transport codes

COCONUT, which consists of the 1.5D core transport code JETTO coupled to the 2D-edge transport code EDGE-2D. JETTO explicitly takes the region of the edge transport barrier into account. It is assumed that anomalous transport is completely suppressed within the ETB, so that the only remaining transport is neo-classical [2]. The width of the ETB is considered an external parameter, which is calculated using recently developed models [3]. Perpendicular transport in the SOL is assumed to be neo-classical as well with longitudinal transport being classical. JETTO has a fixed boundary solver of the Grad-Shafranov equation, which generates equilibrium consistent with predicted pressure and current profiles in the core and ETB. JETTO is linked with the MHD stability code IDBALL, which generates ideal ballooning stability diagrams in s - α co-ordinates. Recently JETTO has been linked with the much more sophisticated MHD stability code MISHKA [4], which includes stability analysis of both finite- n ballooning and kink/peeling modes.

To simulate ELMs, JETTO uses simple analytical formulas, which evaluate ballooning or kink stability inside the separatrix (like $\alpha \leq \alpha_{crit}$ or $j_{ETB} \leq j_0$; these formulas are checked against results from IDBALL and MISHKA). JETTO increases temporarily the level of anomalous transport within the ETB as soon as stability criterion is violated. Both pressure gradient and edge current drop as a result so that plasma returns to a pre-ELM state and the cycle repeats.

1. Modelling of ELMy H-mode with strong gas puffing

As noted above, we have selected the JET shot #53298 as a prototype to study the role of gas puffing in type-I ELMy H-mode performance. Three different levels of gas puffing have been used throughout the simulations: $\Gamma = 0$; 4×10^{22} and 1×10^{23} atoms/sec. We use the COCONUT suite to simulate the time evolution of both core and SOL profiles between ELMs. Figure 2 shows some characteristic profiles for the three reference cases. The inspection of these profiles shows that gas puffing leads to a density rise both in the core and in the SOL. However the density rise near the separatrix is much stronger than in the core. Since we try to keep in the computations the pressure gradient within the ETB roughly the same for all three runs, the lower density gradient in the case with strong gas puffing translates into lower edge temperature. Both these factors lead to a dramatic increase in plasma collisionality for the case of a strong gas puffing. Since the bootstrap current decreases with plasma collisionality, we conclude that strong gas puffing significantly reduces edge current (see Figure 2c). Given the essential role played by edge currents in both kink and ballooning stability, we run the MISHKA code for all three cases. The result of this analysis is presented in Figure 3 and allows us to draw the following conclusions:

- The discharge with no gas puffing enters the second ballooning stability region; its maximum pressure gradient corresponds to $\alpha_{crit} \approx 6$ and is limited by finite- n ballooning modes with radial localisation approximately equal to the width of the ETB;
- Medium level of gas puffing reduces the bootstrap current near the separatrix only. This makes the magnetic surfaces close to the separatrix ballooning unstable but does not deteriorate the critical pressure gradient deeper inside the ETB ($\alpha_{crit} \equiv -\frac{2\mu_0 q^2}{B_0^2 \epsilon} \left(\frac{dp}{d\rho} \right)_{crit} \approx 6$ still holds). It is worth noting that this kind of MHD activity is qualitatively similar to what experimentalists observe in type-II ELMy H-mode between big ELMs [5] or during the EDA mode [6].
- The highest level of gas puffing destroys the bootstrap current across the whole the ETB. The whole edge barrier loses access to a second stability region so that the maximum achievable normalised pressure gradient drops to $\alpha_{crit} \approx 3.5$.

To find out how the ELM frequency depends on the level of α_{crit} , we run JETTO for two cases: with zero gas puffing and maximum gas puffing using the same assumptions about amplitude and structure of ELM but assuming that $\alpha_{crit} \approx 6$ for the no gas case and $\alpha_{crit} \approx 3.5$ for the case with $\Gamma = 1 \times 10^{23} \text{ sec}^{-1}$. The result of this study is shown on Figure 4 and allows us to conclude that qualitatively the transition from the second ballooning stability to first ballooning stability limit

corresponds to a transition from type-I to type-III ELMs (both in terms of ELM frequency and change in confinement).

The next aim of our analysis was to look at the time evolution of plasma parameters while approaching the MHD stability limit. To do it, we assume that the plasma parameters are not limited by any edge MHD instabilities (peeling or ballooning). We monitor the MHD stability of the plasma edge during such unrestricted evolution. Plasma heating leads to an increase in plasma pressure gradient, particularly within the ETB, where transport is reduced to a neo-classical level. This is accompanied by an increase in edge current (both bootstrap and Ohmic) with the corresponding reduction in magnetic shear. As a result, the top-of-the-barrier operational point moves in s - α space so that it crosses the ideal ballooning stability limit before entering the second stability region. We should stress that this kind of evolution is quite typical, in fact it is observed in all the shot we simulated so far.

So if the ETB region crosses the ideal ballooning unstable area before entering the second stability region, then the question arises how can plasma overcome this “primary” instability. Numerical modelling shows that one way to do it would be to avoid unstable region by increasing the edge current without increasing pressure gradient [7]. Indeed this method works, but it requires some special current ramp-up technique only occasionally used in present day experiments. Another way would be to assume that ideal ballooning instability (with $n \Rightarrow \infty$) generates a relatively small incremental transport. If this is the case then plasma can be pushed through the unstable region with the help of “extra” power. We leave the detailed discussion of this idea for the future work and finish this paragraph with only one remark. It is known experimentally that plasma edge passes through a chain of transformations while the heating power is rising. First the L-H transition occurs followed by the type-III ELMy H-mode with the ELM frequency going down with the power. The plasma jumps then into an ELM-free period when more power is applied and finally enters into type-I ELMy H-mode with the ELM frequency rising with power. Qualitatively this chain of transitions is similar to what we found in our simulations: that plasma reaches the first ballooning stability limit after the establishment of the ETB (L-H transition) and stay there if the power is not high enough. This corresponds to a type-III ELMy H-mode. With more power plasma enter the second stability region (ELM-free period) followed by strong type-I ELMy H-mode, caused by finite ballooning and peeling instabilities. It is worth noting that ballooning stability boundary can be controlled by resistive rather than by ideal ballooning mode in highly collisional plasma. Other effects such as diamagnetic terms may affect the stability boundaries as well.

5. Triangularity scan.

We select two recent JET shots, which are identical in all other respects but have different triangularity: #53187 has $\delta \approx 0.3$ and #53298 has $\delta \approx 0.5$. We performed predictive modelling of these two shots with JETTO using the same models for the ETB width [3] and same assumptions about ballooning stability. The modelling confirmed that both low and high triangularity plasmas could enter second stability after passing through the ballooning unstable region with the characteristic width of the unstable region rising with triangularity. Using the same assumption for α_{crit} leads to either to underestimation of the high triangularity plasma energy content or to overestimation of the low triangularity plasma (depending on the level of α_{crit}). To elucidate the situation with MHD stability we generated a range of magnetic configurations with triangularity varying from $\delta \approx 0.1$ to $\delta \approx 0.5$ and performed predictive modelling and full MHD stability analysis of three otherwise identical plasmas with $\delta = 0.1, 0.3$ and 0.5 . Some results of MHD analysis are shown on Figure 5 and allow us to draw the following conclusions. The very low triangularity ($\delta = 0.1$) plasma has no access to a second stability region mainly because of low- n kink/peeling mode. The medium triangularity plasma ($\delta = 0.3$) gets some access to a second stability but this access is very narrow in the s - α space and requires an accurate tailoring of the edge plasma parameters to get into it. Increasing triangularity above $\delta \geq 0.3$ widens the access to the second stability although it increases the maximum level of α_{crit} only slightly (see [8]).

6. Conclusions

Self-consistent integrated modelling of a number of JET type-I ELMy H-mode discharges has been carried out using the suite of JET transport codes COCONUT coupled with the MHD stability codes IDBALL and MISHKA. It has been shown that generally JET plasmas with ETB can get access to second ballooning stability with the critical level of normalised pressure gradient being controlled by medium-n ballooning/peeling modes. Strong gas puffing reduces the edge current and brings the operational point back into the first ballooning stability region. This transition is accompanied by a dramatic increase in ELM frequency similar to experimentally observed transition from type-I to type-III ELMs. Modelling of plasmas with different triangularity reveals that higher triangularity gives better access to a second ballooning stability, which improves plasma performance.

7. Acknowledgements

This work was partly funded by the UK Department of Trade and Industry and by EURATOM and was performed under the European Fusion Development Agreement.

8. References

1. R Sartori, B Balet, S Clement et al., Plasma Phys Control Fusion **40** (1998) p 757 and/or R Sartori, D Borba, G D Conway et al., E Proc. 26 EPS Conf. Contr. Fusion and Plasma Physics, Maastricht, 1999, ECA Vol **23J**, 197-200;
2. V. Parail et al., Proc. 27 EPS Conf. Contr. Fusion and Plasma Physics, Budapest, 2000, ECA Vol **24B**, 61-64;
3. T. Onjun et al., submitted to Phys. Plasmas, 2002;
4. A.B. Mikhailovskii, A.C.C. Huysmans et al., Plasma Phys. Rep. **23**, 844 (1997);
5. G Saibene, R Sartori, A Loarte et al., Plasma Phys Control Fusion **44** (2002);
6. I Hutchinson, R Boivin, P T Bonoli et al., Nuclear Fusion **41** (2001) 1391;
7. P.B. Snyder, H.R. Wilson et al., Phys. Plasmas, **9**, (2002), 2037;
8. G Saibene, L D Horton, R Sartori et al., Nuclear Fusion **39** (1999), p 1133

Figure captions

1. Time evolution of the energy content (a), energy confinement time enhancement factor H_{98Y2} (b) and D_{α} signals for JET shots ##53186, 53298, 53299 and 52739 (c-f);

Figure 2. Edge plasma profiles for a gas scan: ion density (a), ion temperature (b), bootstrap current density (c), current density (d) and magnetic shear (e);

Figure 3. MHD stability (ideal ballooning- blue crosses, finite-n ballooning- dark shaded area, kink/peeling- light shaded area) of the gas scan shots from Figure 3: $\Gamma=0$ (a), $\Gamma=4e22$ (b), $\Gamma=1e23$ (c). Three operational points are shown: just inside ETB, on the top of ETB and a point at $\Psi \approx 0.98 - 0.99$;

Figure 4. Time evolution of top-of-barrier χ_i for $\alpha_{crit}=1$ and 2 (a), thermal energy content (b) and confinement time enhancement factor H_{89} (c) for the shot #53298;

Figure 5. MHD stability of the triangularity scan $\Delta=0.1$ (a), $\Delta=0.3$ (b) and $\Delta=0.6$ (c)

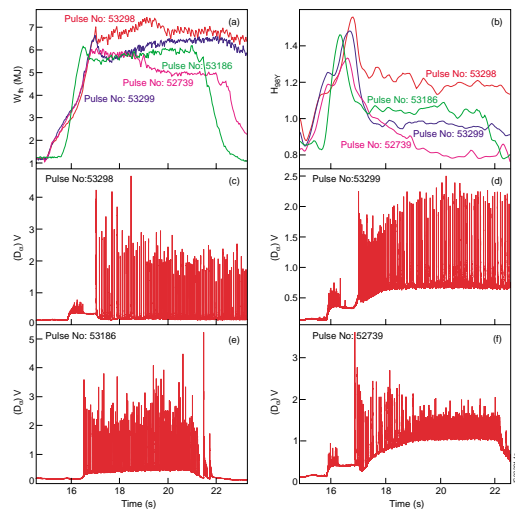


Figure 1

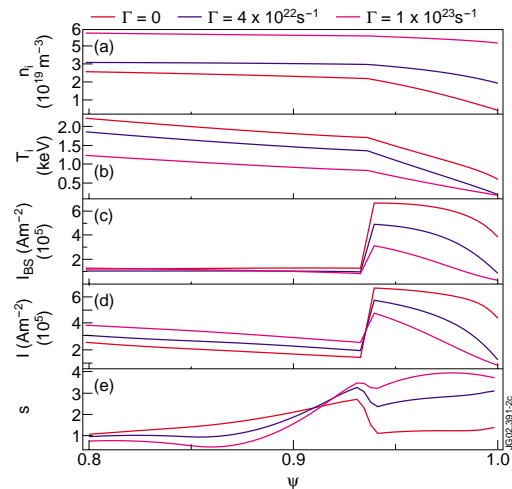


Figure 2

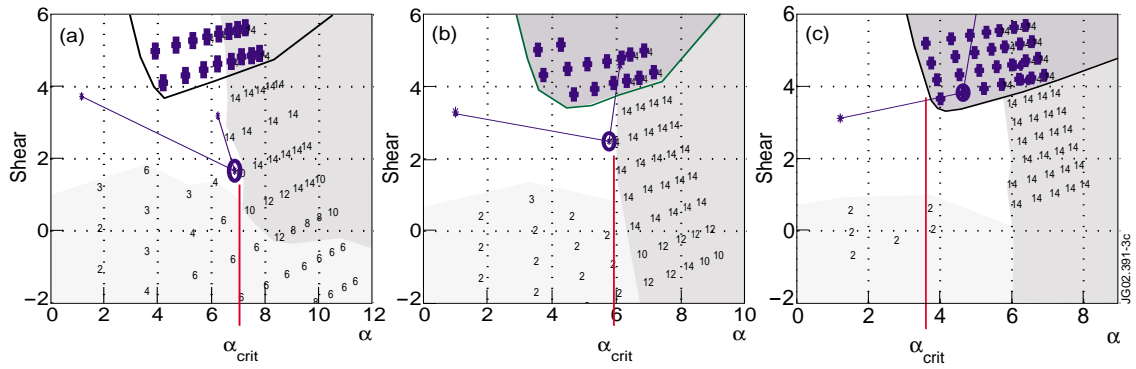


Figure 3

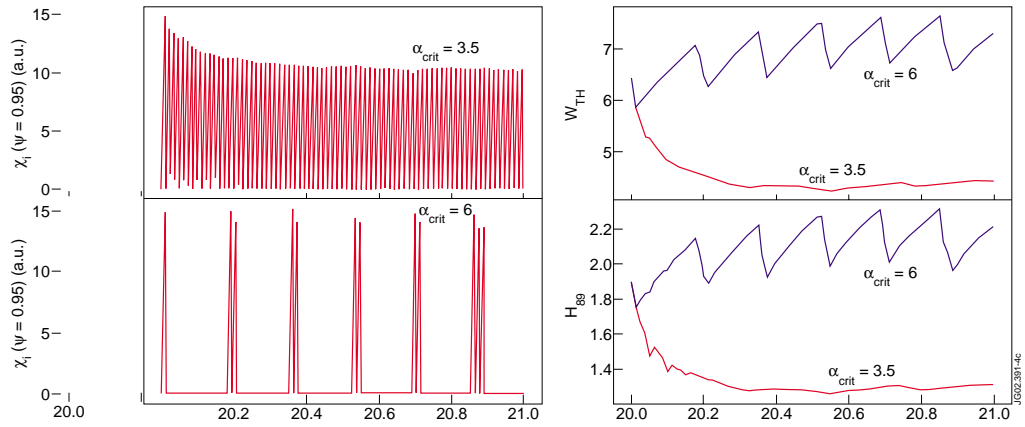


Figure 4

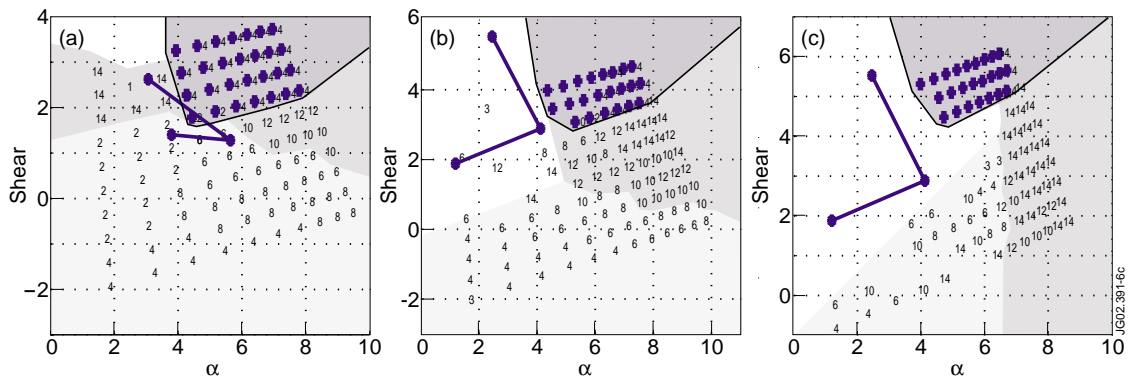


Figure 5